ISSN (Print) 1226-1750
ISSN (Online) 2233-6656
Journal of Magnetics 31(2), 259-268 (2026) https://doi.org/10.4283/JMAG.2026.31.2.259

Magnetic Induction and Heat Transfer Analysis of Carbon Nanotubes Over Curved Surfaces: A Comparative Assessment of Yamada–Ota, Xue, and Tiwari–Das Models

Sami Ullah Khan[1]*, Adnan[2], K. Ramesh[3,4], Kaouther Ghachem[5], Aboulbaba Eladeb[6], Chemseddine Maatki[7], and Lioua Kolsi[8]

[1]*Department of Mathematics, Namal University, Mianwali 42250, Pakistan*
[2]*Department of Mathematics, Mohi-ud-Din Islamic University, Nerian Sharif, 12080, AJ&K, Pakistan*
[3]*Department of Pure and Applied Mathematics, School of Mathematical Sciences, Sunway University, Bandar Sunway, Petaling Jaya, 47500, Selangor Darul Ehsan, Malaysia*
[4]*Department of Mathematics, School of Chemical Engineering and Physical Sciences, Lovely Professional University, Jalandhar, Punjab, India*
[5]*Department of Industrial and Systems Engineering, College of Engineering, Princess Nourah bint Abdulrahman University, P.O. Box 84428, Riyadh, 11671, Saudi Arabia*
[6]*Mining Research Center, Northern Border University, P.O. Box 1321, Arar 91431, Saudi Arabia*
[7]*Department of Mechanical Engineering, College of Engineering, Imam Mohammad Ibn Saud Islamic University (IMSIU), Riyadh 11432, Saudi Arabia*
[8]*Department of Mechanical Engineering, College of Engineering, University of Ha'il, Ha'il City 81451, Saudi Arabia*

(Received 20 November 2025, Received in final form 27 March 2026, Accepted 31 March 2026)

The hybrid nanofluid (HNF) presents superior thermal impact and stability in contrasting to traditional nanofluid, making them more suitable for peak thermal results in thermal systems and solar energy. This investigation presents optimize thermal performances of Casson-micropolar hybrid nanofluid (HNF), containing suspension of single-walled carbon nanotubes (SWCNTs) and multi-walled carbon nanotubes (MWCNTs). The role of base fluid is specified by using ethylene glycol (EG) base fluid. The flow is confined by curved stretched surface. Heat transfer analysis is subject to applications of thermal radiation effects and variable thermal conductivity. A complex system of equations is developed for formulated model which is numerically solved with help of shooting technique. Comparative assessment for heat transfer is addressed for three recognized nanofluid models namely Xue, Tiwari-Das and Yamada-Ota models to examine the prediction for CNT-nanofluid. The results show that the Yamada-Ota model exhibits superior thermal impact as compared to Xue and Tiwari-Das models. The quantitative observations show that the Yamada–Ota model predicts approximately 1-7% higher Nusselt number, based on the flow parameter. However, in case of Tiwari–Das model, the Yamada–Ota model increase the Nusselt number approximately 100-175%, justifying the significance of anisotropic conductivity modeling in carbon nanotubes.

Keywords : carbon nanotubes, variable thermal conductivity, thermal radiation, curved stretching surface, numerical computations

1. Introduction

The nanomaterials are colloidal decomposition generated by nanoscale particles into some base materials. The nanofluids occupies enhanced convective thermal performance and impressive conducting features. These fluids account larger surface area to volume ratio, particle-fluid interaction and interfacial layering which are used to promote the energy transport features. The nanofluids have increasing demand in cooling processes, micro-electronics, modern heat management systems etc. This topic is exclusively studied by various researchers. Nadeem *et al.* [1] analyzed the axisymmetric flow of nanofluid in Riga plate. Alblawi *et al.* [2] accounted the

*Corresponding author: Tel: +92313714665
e-mail: sk_iiu@yahoo.com

Casson nanofluid rheological dynamic and thermal features in both fixed and moving frame of references. Thi *et al.* [3] addressed the formation of ε-Fe_2O_3 Nanoparticles to investigate the heat transfer enhancement. Recent advancements in nanotechnology brought the idea of hybrid nanofluid (HNF), decomposition of two or more different nanoparticles with base liquids. The hybrid nanofluid (HNF) are promising category of nanomaterials with peak thermal features and enhanced energy capacity. The HNF benefit from synergistic interactions within different nanoparticles with leading energy transport impact and high conducting performances. HNF are preferred in solar systems, nuclear systems, thermal collectors, next generation cooling systems etc. The scientists have proposed various HNF models in complex systems to tailor the thermo-physical prospective. The research on HNF is diverse and many researchers has studied thermal prospective of these materials with different flow features. For instance, Abbas *et al.* [4] observed thermal rheology of HNF in nonlinear stretched cylinder subject to inclined magnetic force. Saeed *et al.* [5] observed the boosted thermal impact associated to curved surface flow of HNF with non-inertial effects. Aladdin *et al.* [6] focused to vertical cylinder flow of HNF impacted with thermal radiation features. Acharya *et al.* [7] examined the thermal reflection of heat transfer due to HNF in a micro-wavy channel. Implication of non-classical Fourier model to study heat transfer due to HNF has been predicted by Hayat *et al.* [8]. Rahman *et al.* [9] explored thermal analysis containing titanium oxide and iron nanoparticles in rotating disks. Acharya [10] explored the buoyancy driven flow of multi-walled carbon nanotubes comprises by annular enclosure. The influence of fitted curved fins curvature on flow behavior of hybrid nanofluid with additional impact of entropy generation was predicted by Acharya [11].

Khalatbari *et al.* [12] performed literature review on hybrid nanofluid suspension subject to different thermal features. Research illustrating the buoyancy force of HNF through semi-circular chamber with triangular heater was addressed by Acharya and Öztop [13]. Nayak *et al.* [14] determined the nonlinear radiation effects in assisting of HNF with optimized simulations. Sheikholeslami *et al.* [15] explored thermoelectric power generation subject to HNF via experimental data. Sharma *et al.* [16] accounted the HNF heating impact in conical gap configuration with assessment of shape features. Thermal consideration of silver, cobalt ferrite and titanium dioxide nanoparticles with Darcy media was pronounced by Reddy *et al.* [17]. Venkateswarlu *et al.* [18] explored HNF thermal properties and synthesis under influence of electromagnetic force. Sensitivity analysis in spinning sphere confined by hybrid nanofluid was visualized by Thumma *et al.* [19].

The carbon nanotubes (CNTs) are cylindrical structures, containing carbon atoms arranged in hexagonal lattice. Subject to unique structure, the carbon nanotubes (CNTs) possess exceptional mechanical, thermal and electrical characteristics. CNTs when dispersed in base materials, results a peak conductive nanofluids which attains unique flow behavior under diverse physical constraints. The dynamic of CNTs are impacted with different factors like base fluid features, amplification of magnetic force, electric force, pressure gradients etc. The significance of CNTs are justified in advanced energy systems, high efficiency cooling technologies, microfluidics and several biomedical applications. The CNTs are classified into two basic types like single-walled carbon nanotubes (SWCNTs) and multi-walled carbon nanotubes (MWCNTs). SWCNTs consisting of single layer of graphene rolled structure with diameter 0.4 to 2 nm. On other hand MWCNTs represent the multiple layers structure of graphene arranged within one another. The structure of MWCNTS lies between 2 to 100 nm. Mahmood *et al.* [20] implemented the anisotropic slip insight for study thermal prospective of carbon nanotubes (CNTs) with help of Yamada-Ota model. Bashir *et al.* [21] deduced Darcy–Forchheimer features in CNTs with induction of magnetic force. Samat *et al.* [22] determined thin needle transport of CNTs by proposing numerical and research surface tools. Explanation of CNTs in porous duct following peristaltic phenomenon has been responded by Akbar *et al.* [23]. Naeem *et al.* [24] presented comparative heat transfer results due to CNTs with help of Yamada Ota and Xue models. Results exploring the thermal progressive of CNTs due to curved surface has been studied by Roopa *et al.* [25]. Rajput *et al.* [26] claimed heat transfer due to CNTs with slip effects by computing multiple solutions. Ishtiaq *et al.* [27] simulated non-similar computations for ternary HNF by following the Yamada-Ota and Xue models. Behera *et al.* [28] expressed thermal reputation of HNF in curved surface with porous layer. Shaw *et al.* [29] responded the inertial impact in HNF due to thin needle by using the Buongiorno nanofluid model.

Although the study of carbon nanotubes has been exclusively studied, most existing investigations adopt a single thermo-physical without presenting comparative review of Yamada–Ota, Xue, and Tiwari–Das models. Moreover, comparative thermal aspects of Yamada–Ota, Xue, and Tiwari–Das models through curved surface has not been explored yet. This investigation proposed comparative simulations for flow of carbon nanotubes (CNTs) by employing three famous nanofluid models namely

Yamada-Ota, Xue, and Tiwari-Das models. The carbon nanotubes (CNTs) properties are explored due to suspension of single-walled carbon nanotubes (SWCNTs) and multi-walled carbon nanotubes (MWCNTs) with ethylene glycol (EG). Heat transfer features are addressed by using radiated effects and assumptions of variable thermal conductivity. Numerical data for modeled problem is attained with help of shooting technique. An elastic curved stretched sheet is assumed to generates the flow. Comparative thermal evaluation of heat transfer impact is examined comparatively for Yamada-Ota, Xue, and Tiwari-Das models. The results show new insights into analyzing thermal transport in HNF flow through complex configurations, thermal management in aerospace engineering and solar system.

2. Problem Formulation

Let us assume steady, laminar flow of Casson-micropolar HNF due to curved stretched surface. Let x denotes the radial axis while S be arc length of surface. Denoting the curvature with R_1. Assuming U and W be velocity component along the radial axis and arc length, respectively. Magnetic force is assumed normal to the flow. The wall velocity is defining with U_w, micro-rotation component is surface N, temperature with t_w while T_∞ is associated to ambient temperature. The variable thermal conductivity and thermal radiation consequences are followed in heat equation. Following governing equations have been modeled under such flow constraints [30, 31]:

$$\frac{1}{x+R_1}\left((x+R_1)V\right)_r+\frac{R_1}{x+R_1}(U)_s=0, \tag{1}$$

$$\frac{U^2}{x+R_1}=\frac{1}{\rho_{hnf}}P_r, \tag{2}$$

$$\begin{aligned}V(U)_r+\frac{R_1U}{r+R_1}(U)_s+\frac{UV}{r+R_1}+\frac{1}{\rho_{hnf}}\frac{R_1}{r+R_1}P_r\\=\nu_{hnf}\left[\left(1+\frac{1}{\beta}+k^*\right)\left(U_{rr}-\frac{U}{(r+R_1)^2}+\frac{1}{r+R_1}U_r\right)\right]-\frac{k^*}{\rho_{hnf}}(N)_r\\-\frac{\sigma_{hnf}B_0^{\,2}}{\rho_{hnf}}U,\end{aligned} \tag{3}$$

$$\begin{aligned}V(N)_r+\frac{R_1U}{r+R_1}(N)_s=\frac{\gamma_{hnf}}{\rho_{hnf}j}\left(N_{rr}+\frac{1}{r+R_1}N_r\right)\\-\frac{k^*}{\rho_{hnf}j}\left(2N+U_r+\frac{U}{r+R_1}\right),\end{aligned} \tag{4}$$

$$\begin{aligned}V(T)_r+\frac{R_1U}{r+R_1}(T)_s=\frac{1}{(\rho C_p)_{hnf}}\frac{1}{r+R_1}\left((r+R_1)T_rk_{hnf}(T)\right)_r\\-\frac{1}{x+R_1}\left((x+R_1)q_r\right)_r,\end{aligned} \tag{5}$$

Boundary conditions are [30, 31]:

$$U=U_w,\ V=0,\ T=T_w+\chi_1\frac{k_{hnf}}{k_f}(T)_r,\ N=-n(U)_r \text{ at } r\to 0,$$

$$U=0,\ T=T_\infty,\ N=0, \text{ at } r\to\infty. \tag{6}$$

with Casson fluid coefficient β, vertex viscosity k^*, electrical conductivity σ_{hnf}, HNF density ρ_{hnf}, magnetic field strength, B_0, thermal conductivity k_{hnf}, radiated flux q_r and specific heat $(\rho C_p)_{hnf}$. Table 1 proposed physical quantities of HNF via mathematical expressions.

For micropolar fluid, the rotating gradient viscosity γ_{hnf} is defined by:

$$\gamma_{hnf}=\left(\mu_{hnf}+\frac{k_1}{2}\right)j. \tag{7}$$

with micro-inertia j. Following new variables are defined for simplifying the system [30, 31]:

$$T=T_\infty+e^{\frac{s}{a^*}}(T_w-T_\infty)\theta(\eta),\ \eta=r\sqrt{\frac{b^*e^{\frac{s}{a^*}}}{2\nu_fa^*}},\ \ P=\rho_fb^{*2}e^{\frac{2s}{a^*}}p(\eta),$$

$$N=b^*e^{\frac{3s}{2a^*}}\sqrt{\frac{b^*}{2\nu_fa^*}}g(\eta),\ U=b^*e^{\frac{s}{a^*}}f'(\eta), \tag{8}$$

Table 1. HNF thermal characteristics with help of mathematical relations [28, 29].

Properties	Hybrid nanofluid
Density	$\frac{\rho_{hnf}}{\rho_f}=\phi_1\rho_{s_1}+(1-\phi_1).(1-\phi_2)\phi_2\rho_{s_2}.$
Heat capacity	$\frac{(\rho C_p)_{hnf}}{(\rho C_p)_f}=\phi_1(\rho C_p)_{s_1}+(1-\phi_1)(1-\phi_2)\phi_2(\rho C_p)_{s_2}$
Dynamics Viscosity	$\mu_{hnf}=\frac{\mu_f}{(1-\phi_1)^{2.5}(1-\phi_2)^{2.5}}.$
Thermal Conductivity	$\frac{k_{hnf}}{k_{bf}}=\frac{k_{s_2}+(n-1)k_{bf}-(k_{bf}-k_{s_2})(n-1)\phi_2}{k_{s_2}+(n-1)k_{bf}+(k_{bf}-k_{s_2})\phi_2}$ $\frac{k_{bf}}{k_f}=\frac{k_{s_1}+(n-1)k_f-(k_f-k_{s_1})(n-1)\phi_1}{k_{s_1}+(n-1)k_f+(k_f-k_{s_1})\phi_1}$

$$p' = \frac{(f')^2}{\eta + K}, \tag{9}$$

Simplified system is:

$$\frac{\eta\alpha}{\eta+\alpha}p' + \frac{4\alpha}{\eta+\alpha}p = \frac{\rho_f}{\rho_{hnf}}\left(\frac{1}{(1-\phi_1)^{2.5}(1-\phi_2)^{2.5}} + \gamma + \frac{1}{\beta}\right)$$
$$\left(f''' + \frac{1}{\eta+\alpha}f'' - \frac{1}{(\eta+\alpha)^2}f'\right) + \frac{\alpha}{\eta+\alpha}\left(ff'' + 2f'^2\right) \tag{10}$$
$$-\frac{\alpha}{(\zeta+\alpha)^2}\left(ff' + \eta f'^2\right) - \gamma g' - \frac{\sigma_{hnf}}{\sigma_f}Mf',$$

$$\frac{\rho_f}{\rho_{hnf}}\left(\frac{1}{(1-\phi_1)^{2.5}(1-\phi_2)^{2.5}} + \frac{\gamma}{2}\right)\left(g'' + \frac{1}{\eta+\alpha}g'\right)$$
$$-\gamma\left(2g + f'' + \frac{1}{\eta+\alpha}f'\right) + \frac{\alpha}{\eta+\alpha}gf' - \frac{\alpha}{\eta+\alpha}fg' = 0, \tag{11}$$

$$\frac{k_{hnf}}{k_f}\frac{(\rho C_p)_f}{(\rho C_p)_{hnf}}\frac{1}{P_r}\left(1 + \frac{4}{3}Rd + \varepsilon\theta\right)\left(\frac{1}{\eta+\alpha}\theta' + \theta''\right) + \varepsilon\theta'^2$$
$$+\left(\frac{\alpha}{\eta+\alpha}f\theta' - \frac{\alpha}{\eta+\alpha}2\theta f'\right). \tag{12}$$

with

$$f(0) = 0,\ f'(0) = 1,\ \theta(0) = 1 + \lambda_1\frac{k_{hnf}}{k_f}\theta'(0),\ g(0) = -nf''(0)$$
$$f(\infty) \to 0,\ \ g'(\infty) \to 1,\ \ \theta(\infty) \to 0,\ \ f''(\infty) \to 0, \tag{13}$$

The pressure gradient has been eliminated by using Eq. (9) in Eq. (10) as follows [30, 31]:

$$\frac{\rho_f}{\rho_{hnf}}\left(\frac{1}{(1-\phi_1)^{2.5}(1-\phi_2)^{2.5}} + \gamma + \frac{1}{\beta}\right)$$
$$\left(f^{iv} - \frac{1}{(\eta+\alpha)^2}f'' + \frac{1}{(\eta+\alpha)^3}f' + \frac{2}{\eta+\alpha}f'''\right) + \frac{\alpha}{\eta+\alpha}[ff''']$$
$$+\frac{\alpha}{(\eta+\alpha)^3}[f'f + 2\zeta(f')^2] - \frac{3\alpha}{\eta+\alpha}[f''f'] - \frac{\alpha}{(\eta+\alpha)^2}[f''f + 7(f')^2$$
$$+4\zeta f''f'] + \gamma g'' - \frac{\sigma_{hnf}}{\sigma_f}M\left[\frac{1}{\eta+\alpha}f' + f''\right] = 0, \tag{14}$$

$$\frac{\rho_f}{\rho_{hnf}}\left(\frac{1}{(1-\phi_1)^{2.5}(1-\phi_2)^{2.5}} + \frac{\gamma}{2}\right)\left(g'' + \frac{1}{\zeta+\alpha}g'\right)$$
$$-\gamma\left(2g + f'' + \frac{1}{\eta+\alpha}f'\right) + \frac{\alpha}{\eta+\alpha}gf' - \frac{\alpha}{\eta+\alpha}fg' = 0, \tag{15}$$

$$\frac{k_{hnf}}{k_f}\frac{(\rho C_p)_f}{(\rho C_p)_{hnf}}\frac{1}{P_r}\left(1 + \frac{4}{3}Rd + \epsilon\theta\right)\left(\frac{1}{\eta+\alpha}\theta' + \theta''\right) + \epsilon\theta'^2$$
$$+\left(\frac{\alpha}{\eta+\alpha}f\theta' - \frac{\alpha}{\eta+\alpha}2\theta f'\right) = 0. \tag{16}$$

Here,

$$C_f = \frac{\tau_{rs}}{\rho_{hnf}U_w^2},\ Nu = \frac{sq_w}{k_f(T_w - T_\infty)},\ C_m = \frac{a^* e^{\frac{s}{a^*}}\tau_m}{\rho_{hnf}U_w^2}\tau_{rs} \tag{17}$$
$$= \left\{\frac{\rho_f}{\rho_{hnf}}\left(\frac{1}{(1-\phi_1)^{2.5}(1-\phi_2)^{2.5}} + \gamma + \frac{1}{\beta}\right)\left(U_r + \frac{U}{r+R_1}\right) + k^*N\right\}_{r=0},$$

$$\tau_m = \left\{\frac{\rho_f}{\rho_{hnf}}\left(\frac{1}{(1-\phi_1)^{2.5}(1-\phi_2)^{2.5}} + \frac{\gamma}{2}\right)\left(N_r + \frac{N}{r+R_1}\right)\right\}_{r=0}, \tag{18}$$

$$q_w = -k_{hnf}(\mathrm{T})_{r_{r=0}},$$

Dimensionless form is:

$$C_f Re^{\frac{1}{2}} = \frac{\rho_f}{\rho_{hnf}}\left(\frac{1}{(1-\phi_1)^{2.5}(1-\phi_2)^{2.5}} + \gamma + \frac{1}{\beta}\right)$$
$$\left(f''(0) + \frac{f'(0)}{\alpha} - n\gamma f''(0)\right), \tag{19}$$
$$C_m Re^{\frac{1}{2}} = \frac{\rho_f}{\rho_{hnf}}\left(\frac{1}{(1-\phi_1)^{2.5}(1-\phi_2)^{2.5}} + \frac{k_1}{2}\right)\left(g'(0) - \frac{nf''(0)}{\alpha}\right),$$

$$Nu Re^{\frac{1}{2}} = -\frac{k_{hnf}}{k_f}\left(1 + \frac{4}{3}Rd\right)\theta'(0). \tag{20}$$

with Reynolds number $Re = \frac{a^* e^{\frac{2s}{a^*}}}{\nu_f}$.

3. Three Hybrid Nanofluid Models

In thermal engineering, three famous nanofluid models are defined by Yamada-Ota, Xue and Tiwari-Das models.

3.1. Yamada-Ota Model

Yamada–Ota is based on anisotropic thermal conductivity features of CNTs. This model preserves exceptional axial thermal aspects of CNTs. Mathematical expressions for this model are:

$$\frac{k_{hnf}}{k_{bf}}=\frac{1+\frac{k_{bf}L}{k_{s_2}R}\phi_2^{\,0.2}+\left(1-\frac{k_{bf}}{k_{s_2}}\right)\phi_2\frac{L}{R}\phi_2^{\,0.2}+2\phi_2\left(\frac{k_{s_2}}{k_{s_2}-k_{bf}}\right)\ln\left(\frac{k_{s_2}+k_{bf}}{2k_{s_2}}\right)}{1-\phi_2+2\phi_2\left(\frac{k_{bf}}{k_{s_2}-k_{bf}}\right)\ln\left(\frac{k_{s_2}+k_{bf}}{2k_{bf}}\right)}, \tag{21}$$

$$\frac{k_{bf}}{k_f}=\frac{1+\frac{k_fL}{k_{s_1}R}\phi_1^{0.2}+\left(1-\frac{k_f}{k_{s_1}}\right)\phi_1\frac{L}{R}\phi_1^{0.2}+2\phi_1\left(\frac{k_{s_1}}{k_{s_1}-k_f}\right)\ln\left(\frac{k_{s_1}+k_f}{2k_{s_1}}\right)}{1-\phi_1+2\phi_1\left(\frac{k_f}{k_{s_1}-k_f}\right)\ln\left(\frac{k_{s_1}+k_f}{2k_f}\right)}. \tag{22}$$

3.2. Xue Model

The formulation of Xue model is based on enhancement of thermal conductivity in nanofluid comprising the cylindrical nanoparticles like CNTs.

$$\frac{k_{hnf}}{k_{bf}}=\frac{1-\varphi_2+2\varphi_2\left(\frac{k_{s_2}}{k_{s_2}-k_{bf}}\right)\ln\left(\frac{k_{s_2}+k_{bf}}{2k_{bf}}\right)}{1-\varphi_2+2\varphi_2\left(\frac{k_{bf}}{k_{s_2}-k_{bf}}\right)\ln\left(\frac{k_{s_2}+k_{bf}}{2k_{bf}}\right)}, \tag{23}$$

$$\frac{k_{bf}}{k_f}=\frac{1-\varphi_1+2\varphi_1\left(\frac{k_{s_1}}{k_{s_1}-k_f}\right)\ln\left(\frac{k_{s_1}+k_f}{2k_f}\right)}{1-\varphi_1+2\varphi_1\left(\frac{k_f}{k_{s_1}-k_f}\right)\ln\left(\frac{k_{s_1}+k_f}{2k_f}\right)}. \tag{24}$$

3.3. Tiwari-Das Model

This model is based on implementation of theory of classical nanofluid subject to volume fraction approach by expressing the thermo-physical features as function of nanoparticles concentration.

$$\frac{k_{hnf}}{k_{bf}}=\frac{(n-1)k_{bf}+k_{s_2}-\left(k_{bf}-k_{s_2}\right)(n-1)\varphi_2}{(n-1)k_{bf}+k_{s_2}+\left(k_{bf}-k_{s_2}\right)\varphi_2}, \tag{25}$$

$$\frac{k_{bf}}{k_f}=\frac{(n-1)k_f+k_{s_1}-\left(k_f-k_{s_1}\right)(n-1)\varphi_1}{(n-1)k_f+k_{s_1}+\left(k_f-k_{s_1}\right)\varphi_1}. \tag{26}$$

4. Solution Methodolgy

Numerical simulations for complex modeled system are performed with help of shooting technique. The shooting method is effective numerical scheme which is preferred due to excellent convergence. This solver effectively tackled various nonlinear problems with excellent accuracy. For shooting method, first order system is attained by using appropriate variables:

$$\begin{aligned}&Z(1)=f(\zeta),\ Z(2)=f'(\zeta),Z(3)=f''(\zeta),Z(4)=f'''(\zeta),\\&ZZ1=f^{iv}(\zeta)\end{aligned} \tag{27}$$

$$\begin{aligned}ZZ1=&-\left(\frac{\rho_f}{\rho_{hnf}}\left(\frac{1}{(1-\phi_1)^{2.5}(1-\phi_2)^{2.5}}+\gamma+\frac{1}{\beta}\right)\right)^{-1}\\&\left(\frac{\rho_f}{\rho_{hnf}}\left(\frac{1}{(1-\phi_1)^{2.5}(1-\phi_2)^{2.5}}+\gamma+\frac{1}{\beta}\right)\right.\\&\left(-\frac{1}{(x+\alpha)^2}Z(3)+\frac{1}{(x+\alpha)^3}Z(2)+\frac{2}{x+\alpha}Z(4)\right)\\&+\frac{\alpha}{x+\alpha}\left[Z(1)Z(4)\right]+\frac{\alpha}{(x+\alpha)^3}\left[Z(2)Z(1)+2x\left(Z(2)\right)^2\right]\\&-\frac{3\alpha}{x+\alpha}\left[Z(3)Z(2)\right]-\frac{\alpha}{(x+\alpha)^2}\left[Z(3)Z(1)+7\left(Z(2)\right)^2\right.\\&\left.\left.+4xZ(3)Z(2)\right]+\gamma ZZ2-\frac{\sigma_{hnf}}{\sigma_f}M\left[\frac{1}{x+\alpha}Z(2)+Z(3)\right]\right),\end{aligned} \tag{28}$$

$$Y(5)=g(\zeta),\quad Y(6)=g'(\zeta),\quad YY2=g''(\zeta) \tag{29}$$

$$\begin{aligned}ZZ2=&-\left(\frac{\rho_f}{\rho_{hnf}}\left(\frac{1}{(1-\phi_1)^{2.5}(1-\phi_2)^{2.5}}+\frac{\gamma}{2}\right)\right)^{-1}\\&\left(\frac{\rho_f}{\rho_{hnf}}\left(\frac{1}{(1-\phi_1)^{2.5}(1-\phi_2)^{2.5}}+\frac{\gamma}{2}+\frac{\gamma}{2}\left(\frac{1}{x+\alpha}Z(6)\right)\right.\right.\\&-\gamma\left(2Z(5)+Z(3)+\frac{1}{x+\alpha}Z(2)\right)\\&\left.+\frac{\alpha}{x+\alpha}Z(5)Z(2)-\frac{\alpha}{x+\alpha}Z(1)Z(6)\right),\end{aligned} \tag{30}$$

$$Z(6)=\theta(\zeta),\quad Z(7)=\theta'(\zeta),\quad ZZ3=\theta''(\zeta) \tag{31}$$

$$\begin{aligned}ZZ3=&-\left(\frac{k_{hnf}}{k_f}\frac{(\rho C_p)_f}{(\rho C_p)_{hnf}}\frac{1}{P_r}\left(1+\frac{4}{3}N+\varepsilon Z(7)\right)\right)^{-1}\\&\left(\frac{k_{hnf}}{k_f}\frac{(\rho C_p)_f}{(\rho C_p)_{hnf}}\frac{1}{P_r}\left(1+\frac{4}{3}N+\varepsilon Z(7)\right)\left(\frac{1}{x+\alpha}Y(8)\right)+\varepsilon Z(8)^2\right.\\&\left.+\left(\frac{\alpha}{x+\alpha}Z(1)Z(8)-\frac{\alpha}{x+\alpha}2Z(7)Z(2)\right)\right).\end{aligned} \tag{32}$$

$$Z(1);\ Z(2)-1;\ Z(7)-1-\lambda_1\frac{k_{hnf}}{k_f}Z(8);\ Z(5)+nZ(3). \tag{33}$$

Table 2. Comparing numerical findings with results of Abbas *et al.* [32] for $-f''(0)$ when $M = 0.2$.

α	Abbas *et al.* [32]	Present results
5	1.22881	1.22884
20	1.07541	1.07543
50	1.04849	1.04850
100	1.03982	1.03983

$$Zinf(1);\ Zinf(6)-1;\ Zinf(7);\ Zinf(3). \qquad (34)$$

A reliable solution accuracy is confirmed with 10^{-6}. The iterations of performed by maintaining the step size of $\Delta\eta = 0.002$. After a finite truncation domain η_∞ is adjusted beyond $\eta_\infty = 12$. The CPU time for computations is 5 to 20 seconds depending upon choice of parameters. Table 2 proposed the validity of results by comparing simulated findings of Abbas *et al.* [32] for limiting case. The calculated results confirm great accuracy with this analysis which ensure the solution validity.

5. Results and Discussion

Physical interpretation of problem is associated to variation of flow parameters. Comparative simulations are presented for Yamada-Ota model, Xue and Tiwari-Das model. Fig. 1(a) incorporates the results for curvature parameter α on velocity profile f'. Subject to increasing variation of α, the velocity profile gets enhancing trend. The source of curvature parameter α is associated to curved surface flow, quantifying the features of geometric curvature on assessment of fluid behavior. Larger change in α characterizes the bending of curved surface which results in enhancement of fluid velocity. The improvement in f' is slower for Tiwari-Das model. The augmentation in velocity profile is larger for Yamada-Ota model. The variation of f' against micropolar fluid parameter γ has been revealed in Fig. 1(b). A depletion in f' is observed due to γ. The results for Casson fluid parameter β is privileged in Fig. 1(c). The velocity profile reduces for β. The reduction in velocity is physically associated to shear thinning and thickening features.

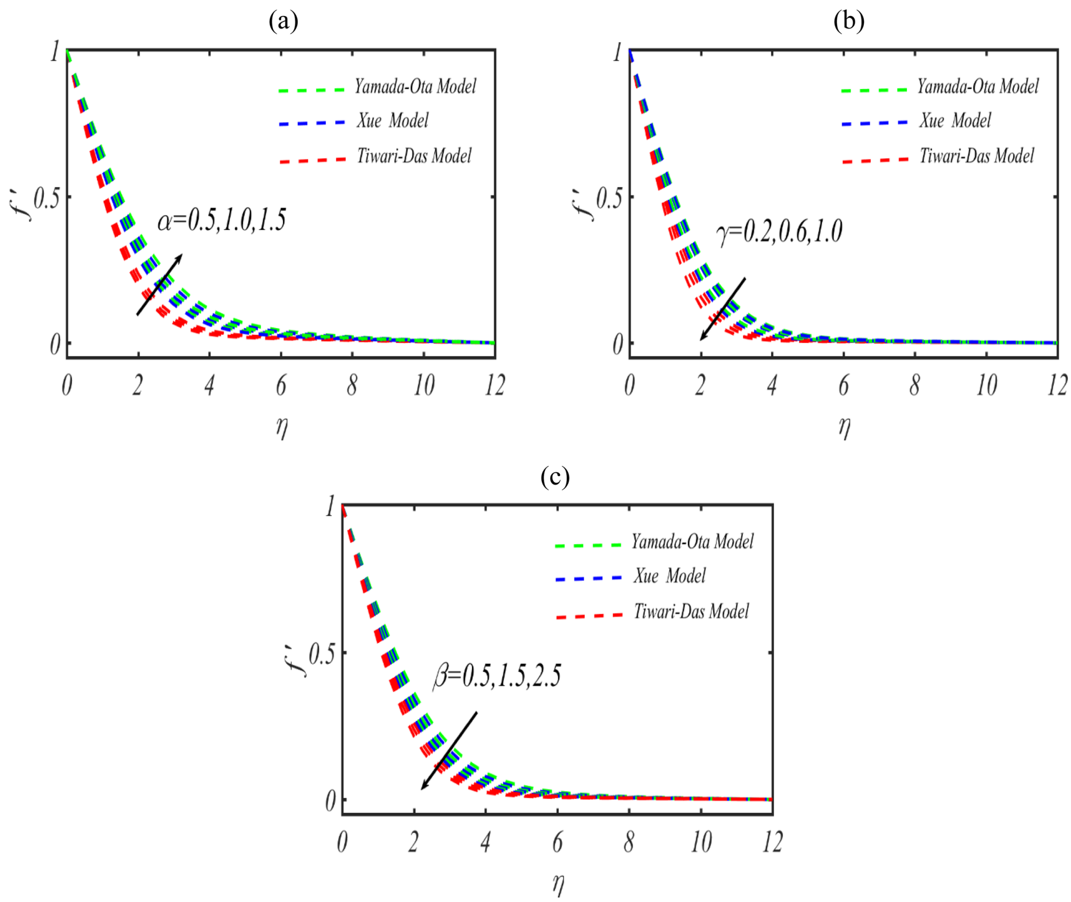

Fig. 1. (Color online) (a-c) Analysis for f' due to (a) α (b) γ and (c) β.

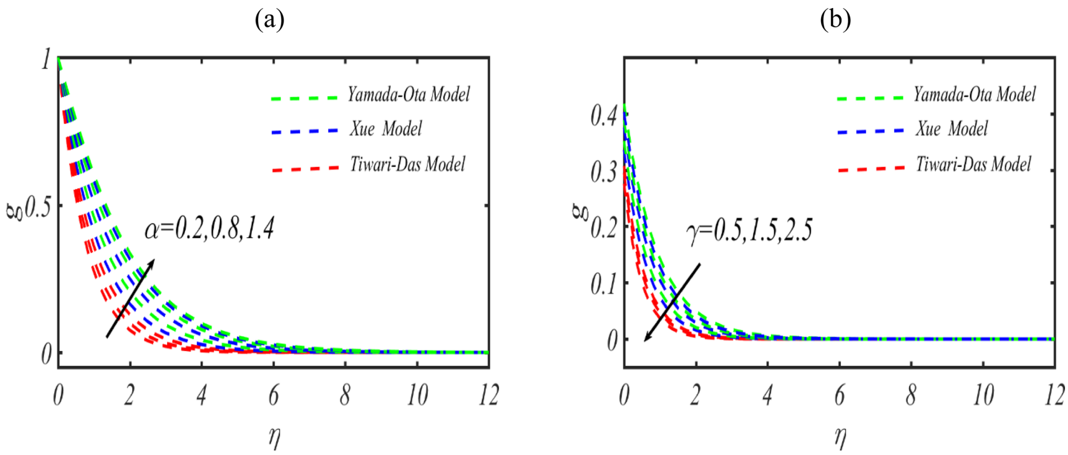

Fig. 2. (Color online) (a-b) Variation of micro-rotation velocity g for (a) α (b) γ.

Fig. 2(a-b) complies the simulations for micro-rotation velocity g due to curvature parameter α and micropolar fluid parameter γ. An increasing change in g have been revealed for α while declining impact in velocity change has been observed for γ.

Fig. 3(a) presents the analysis for temperature profile θ by enhancing variable thermal conductivity parameter ε. The heat transfer boosted with assumptions of variable thermal conductivity. The enhancement in thermal profile is more progressive for Yamada-Ota model. The consideration of variable thermal conductivity is important in various engineering systems where fluid is used as an energy source. Fig. 3(b) incorporates the importance of curvature parameter α on profile of θ. The depicted results showing a decrement in θ due to higher α. Fig. 3(c) justifies the physical aspects of micropolar fluid coefficient γ. The heat transfer enhances for enhancing values of γ. The improvement in heat transfer is relatively larger for Yamada-Ota model. In order to predicts the influence of radiation parameter Rd on θ, Fig. 3(d) is prepared. The radiation parameter predicts relative contribution of thermal radiation to the heat transfer system. The presence of radiative phenomenon leads to enhancement of thermal profile. Such observations account special applications in solar systems, heat exchangers, nuclear reactors, solar collectors and combustion systems. In order to assess the consequences of Casson parameter β on θ, Fig. 3(e) is sketched. An enhanced thermal results for heat transfer have been visualized β. Physically, higher β is associated to low shear rate which facilitates the convective heat transfer process.

Table 3 presents the comparative numerical variation for skin friction coefficient $Re_s^{1/2}C_f$ for Yamada-Ota, Xue and Tiwari-Das models. Firstly, it has been clearly observed that the numerical values for Yamada-Ota and Xue are almost identical. The skin friction enhances due to micropolar fluid parameter (β), Casson fluid coefficient (β) and nanoparticles volume fraction (φ_1, φ_2). However, change in curvature parameter shows reverse results on wall shear force for these nanofluid models. The numerical justification of Nusselt number for Yamada-Ota, Xue and Tiwari-Das models by varying flow parameters have been revealed in Table 4. The Nusselt number enhances due to radiation parameter Rd and thermal Biot number λ_1 while opposite results are associated to leading values of Hartmann number M. The variation in Nusselt number is slower for Tiwari-Das model. It has been noticed that Yamada–Ota model incorporates peak higher numerical values of Nusselt number as compared to Tiwari–Das and Xue models. Such impressive increment can be attributed to distinct formulation of the effective thermal conductivity in Yamada–Ota model, which accounts the peak axial conductivity and elongated cylindrical structure of CNTs. The Yamada–Ota model attributes the anisotropic heat transfer dynamic due to one-dimensional configuration of carbon nanotubes. The tabular structure of carbon nanotubes enhances the axial thermal conduction in base material, leading to boosted thermal diffusion.

6. Conclusions

Following observations are deduced from current analysis:

- The velocity profile gradually increases due to curvature parameter. The improvement in velocity is more prominent for Yamada-Ota model.
- Change in micro-rotation parameter, Casson fluid parameter and micropolar fluid coefficient effectively declined the velocity profile.

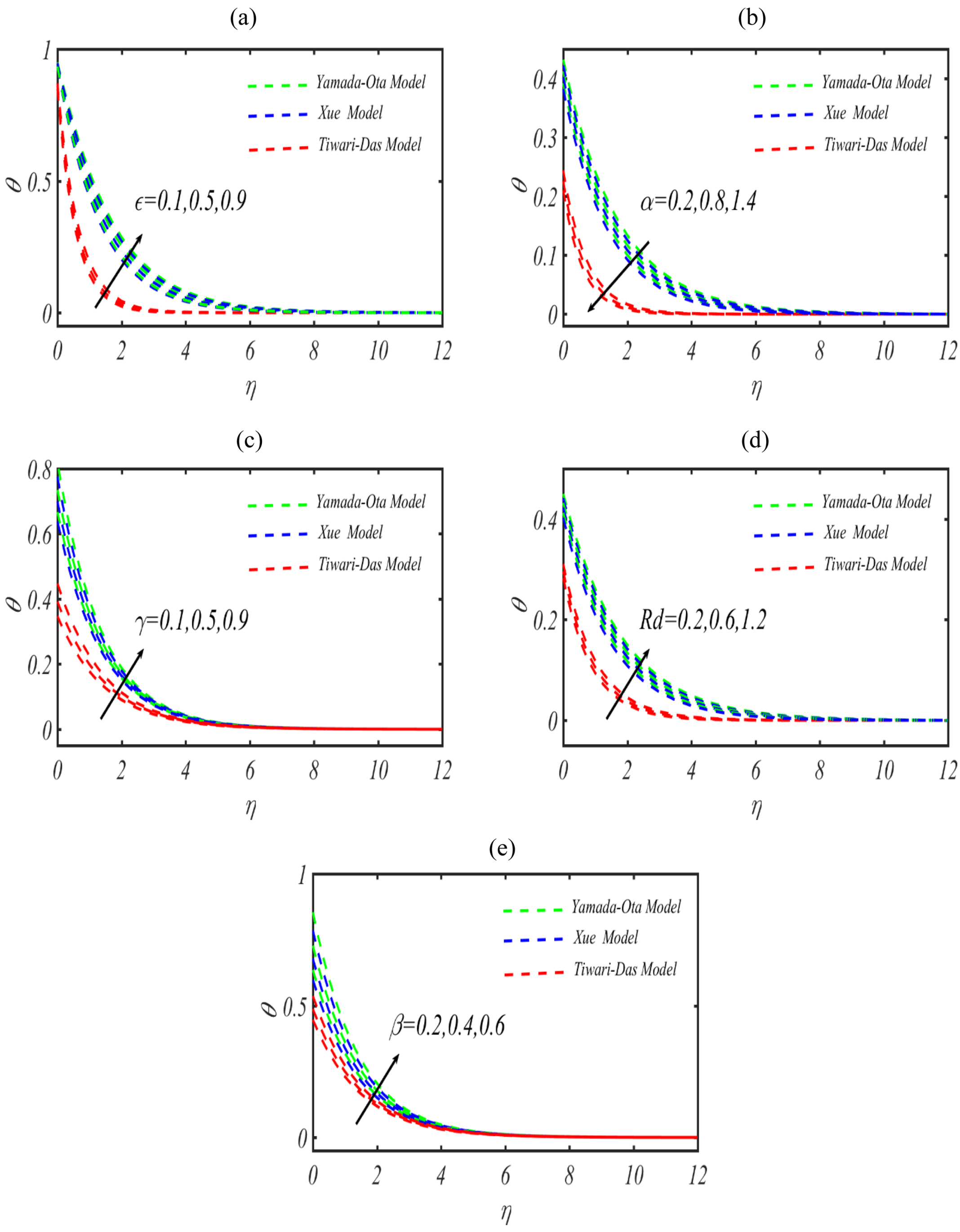

Fig. 3. (Color online) (a-e) Variation of θ for (a) ε (b) α (c) γ, (d) Rd and (e) β.

- The heat transfer enhances with assumptions of variable thermal conductivity, more progressively for Yamada-Ota model.
- Change in Casson fluid parameter and radiation constant increases the heat transfer impact. The enhancement in thermal profile is slower for Tiwari-Das model. Such results important for cooling processes and heat control systems.
- A decrement in heat transfer is exhibited for curvature parameter while increasing results are noted for micropolar fluid constant.
- The Nusselt number declined for Casson fluid parameter, Hartmann number and variable thermal conductivity coefficient. The depletion in Nusselt number is lower for Tiwari-Das model.
- It has been further observed that the Yamada-Ota

Table 3. Numerical variation of $Re_s^{1/2}C_f$ for Yamada-Ota, Xue and Tiwari-Das models.

α	γ	M	β	$\varphi_1 = \varphi_2$	Yamada-Ota model	Xue model	Tiwari-Das model
0.1	0.2	0.4	0.2	0.02	2.6787	2.6779	1.9954
0.3					2.6329	2.6326	1.9207
0.5					2.5786	2.5780	1.8893
0.7					2.5538	2.5529	1.8264
0.2	0.1				2.5901	2.5895	1.7965
	0.5				2.6499	2.6483	1.8590
	0.9				2.6970	2.6966	1.8720
	1.3				2.7437	2.7431	1.8892
		0.3			2.5175	2.5171	1.8136
		0.7			2.4955	2.4953	1.7629
		1.1			2.4681	2.4678	1.7254
		1.5			2.4186	2.4183	1.6874
			0.3		2.6639	2.6636	1.8620
			0.5		2.6822	2.6820	1.8978
			0.7		2.6984	2.6983	1.9354
			0.9		2.7261	2.7258	1.9672
				0.01	2.6935	2.6933	1.7821
				0.03	2.7178	2.7173	1.8063
				0.05	2.7265	2.7262	1.8142
				0.07	2.7391	2.7388	1.8354
				0.09	2.7607	2.7603	1.8457

Table 4. Numerical variation of $Re_s^{1/2}Nu_s$ for Yamada-Ota, Xue-Model and Tiwari-Das models.

Rd	M	$\varphi_1 = \varphi_2$	λ_1	β	ε	Yamada-Ota model	Xue model	Tiwari-Das model
0.1	0.4	0.02	0.4	0.6	0.8	1.7979	1.7769	0.7737
0.5						1.8567	1.8554	0.8503
0.9						1.9129	1.9120	0.9136
1.5						1.9845	1.9736	0.9856
0.6	0.1					1.6879	1.6867	0.7523
	0.3					1.6542	1.6536	0.7328
	0.5					1.6393	1.6387	0.7398
	0.9					1.6158	1.5742	0.7284
		0.01				1.8425	1.8412	0.6687
		0.03				1.8620	1.8516	0.6985
		0.05				1.8879	1.8673	0.7549
		0.07				1.9345	1.9009	0.7928
			0.3			1.7965	1.6875	0.6874
			0.5			1.8582	1.7696	0.7254
			0.7			1.8965	1.8608	0.7554
			0.9			1.9353	1.8932	0.7950
				0.1		1.7245	1.6854	0.71254
				0.5		1.7374	1.6943	0.7354
				1.1		1.7585	1.7357	0.7654
				1.5		1.8032	1.7642	0.7985
					0.3	1.8574	1.8245	0.8844
					0.7	1.8157	1.7854	0.7685
					1.1	1.7658	1.7425	0.7155
					1.7	1.6785	1.7168	0.6792

model shows more impressive thermal results as compared to Tiwari-Das and Xue nanofluid models.

- The extension in this model can be suggested by involving the shape features, bioconvection, entropy generation and machine learning simulations.

Acknowledgments

Princess Nourah bint Abdulrahman University Researchers Supporting Project number (PNURSP2026R41), Princess Nourah bint Abdulrahman University, Riyadh, Saudi Arabia.

References

[1] S. Nadeem, B. Ishtiaq, S. Almutairi, and H. A. Ghazwani, Int. J. Mod. Phys. B **36**, 2250205 (2022).
[2] A. Alblawi, S. Nadeem, M. Zahra, B. Ishtiaq, J. Alzabut, and A. AlZubaidi, ZAMM-Journal of Applied Mathematics and Mechanics/Zeitschrift für Angewandte Mathematik und Mechanik **105**, e70207 (2025).
[3] T. N. Thi, P. C. Van, K. Artavazd, C. Hwang, H. Kim, and J. Jeong, J. Magn. **28**, 239 (2023).
[4] N. Abbas, S. Nadeem, A. Saleem, M. Y. Malik, Alibek Issakhov, and Fahd M. Alharbi, Chinese Journal of Physics **69**, 109 (2021).
[5] A. Saeed, W. Alghamdi, S. Mukhtar, S. I. A. Shah, P. Kumam, T. Gul, S. Nasir, and W. Kumam, Plos One **16**, 0249434 (2021).
[6] N. A. L. Aladdin, Norfifah Bachok, Haliza Rosali, Nadihah Wahi, Nor Aliza Abd Rahmin, and Norihan Md Arifin, Mathematics **10**, 3551 (2022).
[7] N. Acharya, Mater. Today Commun. **38**, 107844 (2024).
[8] T. Hayat, A. Fatima, K. Muhammad, and A. Alsaedi, Materials Science and Engineering: B **288**, 116150 (2023).
[9] M. Rahman, M. Turkyilmazoglu, and Z. Mushtaq, Applied Mathematics and Mechanics **45**, 373 (2024).
[10] N. Acharya, Appl. Therm. Eng. **269**, 126100 (2025).
[11] N. Acharya, Journal of Energy Storage **100**, 113638 (2024).
[12] S. Khalatbari, P. Jalili, B. Jalili, and D. D. Ganji, Proceedings of the Institution of Mechanical Engineers, Part E: Journal of Process Mechanical Engineering, 09544089251318785 (2025).
[13] Acharya, Nilankush, and Hakan F. Öztop manage. Numerical Heat Transfer, Part A: Applications **86**, 1642 (2025).
[14] M. K. Nayak, F. Mabood, A. S. Dogonchi, K. M. Ramadan, I. Tlili, and W. A. Khan, Waves in Random and Complex Media **35**, 1389 (2025).
[15] M. Sheikholeslami, N. Ataollahi, P. Scardi, and M. A. Malagutti, Solar Energy Materials and Solar Cells **285**, 113508 (2025).
[16] J. P. Sharma, R. Kumar, S. V. Easwaramoorthy, and U. Moorthy, Results in Engineering **26**, 104555 (2025).
[17] M. G. Reddy, Gnaneswara, K. Bhagya Swetha Latha, D. Tripathi, O. Anwar Bég, S. Kuharat, and Martin L. Burby, Numerical Heat Transfer, Part A: Applications **86**, 3261 (2025).
[18] B. Venkateswarlu, P. M. Reddy, P. V. S. Narayana, S. W. Joo, and S. A. Alshehri, Journal of the Indian Chemical Society **102**, 101892 (2025).
[19] T. Thumma, Q. M. Al-Mdallal, A. Dawar, S. Ontela, and N. K. Reddy, Alex. Eng. J. **117**, 311 (2025).
[20] Z. Mahmood, K. Rafique, Adnan, U. Khan, T. Muhammad, and A. M. Hassan, Engineering Applications of Computational Fluid Mechanics **18**, 2309139 (2024).
[21] S. Bashir, I. M. Almanjahie, M. Ramzan, A. N. Cheema, M. Akhtar, and F. Alshahrani, Heliyon **10**, e24718 (2024).
[22] N. A. A. Samat, N. Bachok, and N. Md Arifin, Ain Shams Engineering Journal **15**, 102833 (2024).
[23] N. S. Akbar, J. Akram, M. F. Hussain, E. N. Maraj, and T. Muhammad, Mod. Phys. Lett. B **38**, 2450333 (2024).
[24] A. Naeem, Z. Abbas, and M. Y. Rafiq, International Journal of Thermofluids **26**, 101075 (2025).
[25] K. R. Roopa, M. V. Govindaraju, P. A. Dinesh, and S. Yadav, Heat Transfer **54**, 2093 (2025).
[26] S. Rajput, K. Bhattacharyya, A. K. Verma, M. S. Mandal, A. J. Chamkha, and D. Yadav, Waves in Random and Complex Media **35**, 4593 (2025).
[27] B. Ishtiaq, N. A. Ahammad, E. Alshaban, and M. A. Elkotb, Case Stud. Therm. Eng. **74**, 106893 (2025).
[28] S. Behera, S. R. Mishra, P. K. Pattnaik, and Subhajit Panda, Pramana **98**, 151 (2024).
[29] S. Shaw, M. Ijaz Khan, M. K. Nayak, J. K. Madhukesh, R. S. Varun Kumar, Shahid Farooq, and M. Y. Malik, J. Magn. **26**, 363 (2021).
[30] V. K. Narla, C. Biswas, and G. A. Rao, AIP Conference Proceedings **2246**, 020099 (2020).
[31] A. Ashraf, Z. Zhang, T. Saeed, H. Zeb, and T. Munir, Nanomaterials **12**, 1152 (2022).
[32] Z. Abbas, M. Naveed, and M. Sajid, Journal of Engineering Thermophysics **22**, 337 (2013).